Evaluation of Sample Spin-Polarization From Spin-Polarized Scanning Tunneling Spectroscopy Experiments

T.K. YAMADA,[1,2]* A.L. VÁZQUEZ DE PARGA,[3] M.M.J. BISCHOFF,[1] T. MIZOGUCHI,[2] AND H. VAN KEMPEN[1]
[1]*Institute for Molecules and Materials, Radboud University Nijmegen, Toernooiveld 1, 6525 ED Nijmegen, The Netherlands*
[2]*Department of Physics, Faculty of Science, Gakushuin University, 1-5-1 Mejiro, Tokyo, Japan*
[3]*Departamento de Física de la Materia Condensada e Instituto de Ciencia de Materiales "Nicolás Cabrera," Universidad Autónoma de Madrid, Cantoblanco 28049, Madrid, Spain*

KEY WORDS antiferromagnetic coupling; manganese; iron; screw dislocation; tip magnetization

ABSTRACT Spin-polarized scanning tunneling microscopy has produced a great amount of images presenting magnetic contrast between different magnetic domains with an unsurpassed spatial resolution but getting values like the surface polarization has proven to be a difficult task. We will discuss in detail how to extract this information for the case of manganese layers grown on Fe(001) whiskers. Mn layers adopt a body-centered-tetragonal (bct) structure when they are grown on the Fe(001) surface at room temperature. The Mn layers show an antiferromagnetic coupling between the layers. Comparing our spin-polarized scanning tunneling spectra measured with Fe-coated W tips with spin-resolved band structure calculations, we are able to find the value of the sample surface polarization. Also discussed is a method to change the tip magnetization. Finally, the magnetic structure around a screw dislocation on the surface is reviewed. *Microsc. Res. Tech. 66:93–104, 2005.*

INTRODUCTION

Since its invention by Binnig et al. (1982), the scanning tunneling microscope (STM) has revolutionized surface physics research due to its unprecedented spatial resolution combined with its spectroscopic capabilities. Very soon after, there were some first attempts to develop an STM with spin sensitivity. The knowledge about the magnetic structures on very small scales is believed to be crucial for the fundamental understanding of micromagnetism and the controlling of magnetic media and devices in the future. To overcome the obstacles of the established magnetic imaging techniques, the development of the spin-polarized scanning tunneling microscope (SP-STM) to map the spin structure at surfaces down to the atomic level has been the aim of many studies in the past. An instrument with this high resolution would offer fundamentally new insights into the real space order of antiferromagnets, ferromagnets, and ferrimagnets at irregular defects such as dislocations, steps, or atomic point defects, which are inaccessible to scattering techniques, or the transmission of spin-polarized electrons across ferromagnetic/nonferromagnetic interfaces.

The first SP-STM experiments in ultra-high vacuum (UHV) on a clean and well-characterized surface were done by Wiesendanger et al. (1990) using a CrO_2 tip. Since then, several experimental approaches to perform SP-STM measurements have been proposed (Alvarado and Renaud, 1992; Bode et al., 1998; Prins et al., 1996; Suzuki et al., 1997; Vázquez de Parga and Alvarado, 1994; Wulfhekel and Kirschner, 1999). The more successful approach so far is the one proposed by Bode et al. (1998). In this approach, a clean tungsten tip is covered with a layer of magnetic material (ferromagnetic or antiferromagnetic) and the tunneling current depends on the relative orientation of the magnetization of tip and sample. With this method, it has been possible to take images of magnetic structures down to the atomic level (Heinze et al., 2000) surpassing the lateral resolution of any other magnetic sensitive technique. The main limitation in the SP-STM experiments until now is that it is very difficult to obtain quantitative information about the surface magnetism. In this article, we will discuss how to overcome this difficulty using as sample Mn layers grown on an Fe(001) whisker. We will compare our spin-polarized spectra measured with the STM with spin-resolved band structure calculations in order to find the polarization of the sample surface. We will also discuss in detail an experimental procedure to change the tip magnetization. Finally, we will discuss the magnetic structure of the Mn layers around a screw dislocation present on the surface. Comparing the results obtained for the flat areas of the Mn films with the ones obtained around the screw dislocation, we are able to determine the magnetization directions on the surface.

EXPERIMENTAL PROCEDURES

STM and scanning tunneling spectroscopy (STS) measurements were performed in UHV ($\sim 5 \times 10^{-11}$ mbar) at room temperature (RT). The UHV chamber is equipped with a cylindrical mirror analyzer that allows

*Correspondence to: Dr. T.K. Yamada, Department of Physics, Faculty of Science, Gakushuin University, 1-5-1 Mejiro, Toshima-ku 171-8588, Tokyo, Japan. E-mail: toyokazu.yamada@gakushuin.ac.jp

Received 30 September 2004; accepted in revised form16 December 2004

Contract grant sponsor: Ministerio de Educación y Ciencia; Contract grant number: FIS2004-01026; Contract grant sponsor: JSPS Fellows; Contract grant sponsor: International Research Center for Experimental Physics (IRCEP) at the Queen's University, Belfast, Ireland; Contract grant sponsor: Stichting voor Fundamenteel Onderzoek der Materie (FOM).

DOI 10.1002/jemt.20149

Published online in Wiley InterScience (www.interscience.wiley.com).

us to do Auger electron spectroscopy measurements, ion gun, sample and tip heating facilities, low-energy electron diffraction optics (LEED), and different evaporators cooled with liquid nitrogen that allow us to deposit material on the sample or tip, keeping the pressure below 5×10^{-10} mbar.

An Fe(001) whisker was used as a substrate and was cleaned by cycles of Ar^+ sputtering (750 eV) and annealing (up to 730°C). After this cleaning process, around 1% oxygen contaminants were measured by Auger spectroscopy and also in atomically and chemically resolved STM images.

In order to produce a clean Mn(001) surface, about 7 mono-layers (ML) of Mn (purity 99.999%) were grown on the Fe(001) whisker, which was kept at 370 K. The evaporation rate was 0.06 nm/min. After the deposition, more than two Mn layers were exposed on the surface. Using atomically and chemically resolved STM images, we determined that the level of contaminants was below 1% on the Mn surface. Mn layers grown on Fe(001) have a bct structure with the same in-plane lattice constant as Fe(001) and an interlayer distance of 0.165 nm (Yamada et al., 2002).

In this study, we use W tips that were prepared as follows. A W polycrystalline wire (purity 99.99%) with a diameter of 0.5 mm was chemically etched with 5 M KOH aq., then washed with distilled water and introduced in UHV. Once in UHV, the tips were sputtered with Ar^+ (1 kV) and heated by electron-bombardment (2300 K). After this procedure, a clean and blunt W tip is produced.

To get spectroscopic information from the sample surface, STS measurements were performed at every pixel of a constant current topographic image by opening the feedback loop. In a typical measurement, the STM tip stays at every pixel around 100 ms. During 20 ms, the feedback loop is connected and the tip height is recorded to construct the topographic image. During 80 ms, the feedback loop is disconnected and the tunneling current as function of the bias voltage is measured. The voltage range explored was from −2 V up to +3 V with a voltage step of at least 25 mV. The dI/dV curves were obtained by numerically differentiation of the $I(V)$ curves.

THEORETICAL MODEL

STM is based on the quantum mechanical tunnel effect. The first and most simple approximation to get a quantitative understanding of the STM is a one-dimensional model. Let's consider two metallic electrodes (tip and sample) separated by a vacuum gap of a few ångstroms. We will assume that the work function of both metals is identical, that their electronic states can be described in terms of a free electron gas and the temperature is 0 K. The probability density of an electron of one electrode to be located at the position of the other, i.e., at $z = d$ with d being the barrier width, is given by the square of its wave function:

$$w = |\Psi(d)|^2 = |\Psi(0)|^2 \exp(-2\kappa d)$$

The tunneling current flowing between both electrodes is proportional to the sum of all electron states available within the energy interval relevant for tunneling:

$$I(d,V) \propto \exp(-2\kappa d) \sum_{E_i = E_F - eV}^{E_F} |\Psi_i(0)|^2$$

The sum is taken over the different electronic states i of one of the electrodes and the energy interval is set by the voltage applied between the electrodes. This equation is expressed in terms of the local density of states (LDOS) by replacing the summation over discrete states by energy integration:

$$I(d,V) \propto \int_{E_F - eV}^{E_F} dE \sum_i \delta(E_i - E)|\Psi_i(d)|^2 = \int_{E_F - eV}^{E_F} n(d,E)dE$$

The quantity $n(d,E)$ is the LDOS of one electrode at the position d of the other. If we differentiate the previous equation with respect to the energy, we see that the differential conductivity (dI/dV) is related to the LDOS of one of the electrodes:

$$\frac{dI}{dV}(d,V) \propto n(d, E_F + eV)$$

In the 1960s, Bardeen (1961) developed a theoretical method for treating more realistic the tunneling process between two planar electrodes. The basic idea was that the interaction between the electrodes was very weak and the electronic structure of both can be calculated independently. Following this approach, the tunneling current between two weakly bounded electrodes using first-order perturbation theory is:

$$I(z,V) = \frac{2\pi e}{\hbar} \sum_{t,s} |M_{t,s}|^2 \delta(E_t - E_s)[f(E_t - eV) - f(E_s)]$$

where V is the sample bias voltage, z is the tip-sample separation, $M_{t,s}$ is the tunneling matrix element between states of the tip and of the sample, $f(E)$ is the Fermi-Dirac function and E_t and E_s are the energy of the states on the tip and sample, respectively. In the semi-classical WKB approximation, the density of the tunneling current between two planar electrodes can be written as follows:

$$J(z,V) \cong \frac{2\pi e}{\hbar} \left(\frac{\hbar^2}{2m}\right)^2 \int_{-\infty}^{\infty} T(z,V,E)[f(E - eV) - f(E)]\rho_s(E)\rho_t(E - eV)dE$$

where $T(z,V,E)$ is the tunneling transmission probability, $\rho_s(E)$ and $\rho_t(E)$ are the sample and tip density of states, respectively. For low surface temperature the expression for the density of tunneling current can be written as follows:

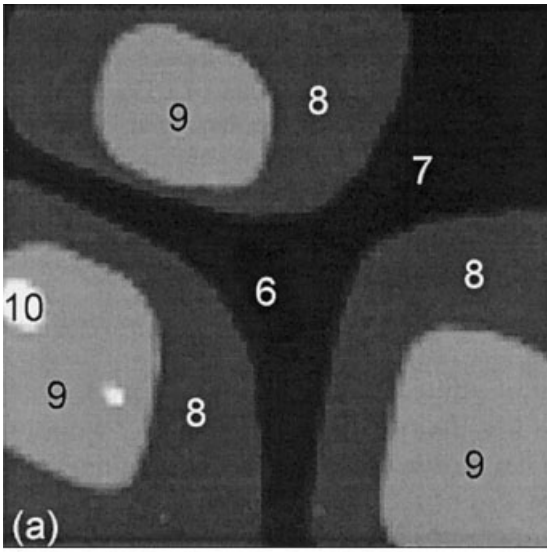

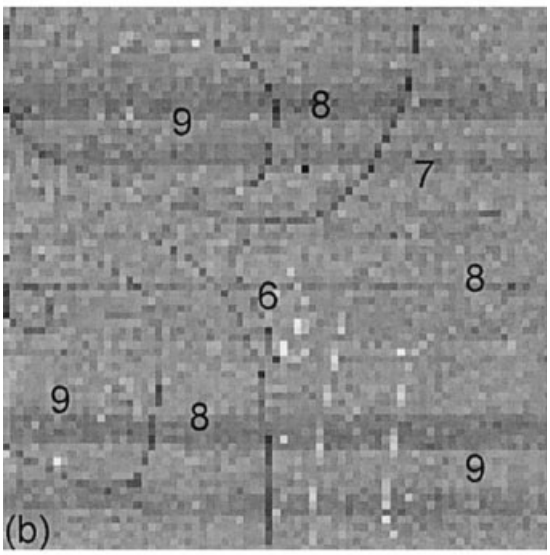

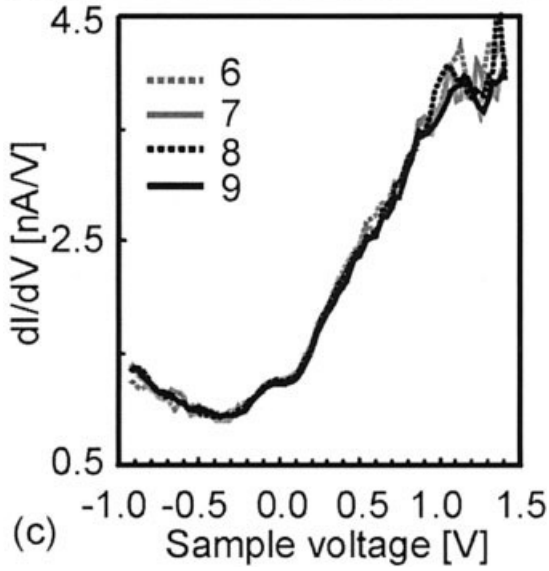

Fig. 1. STS measurement on Fe(001) covered with 7.2 ML Mn at 370 K. (**a**) Topographic image obtained at a set point of $V_s = -0.5$ V, I = 0.5 nA. Scan size is 150 × 150 nm^2. Five different levels are exposed on the surface. (**b**) The dI/dV map at +0.2 V measured at the same area as a. Numbers in a and b denote the stacking number of the Mn layers. (**c**) The dI/dV curves representative of each level. These curves are averages of typically 10 single curves.

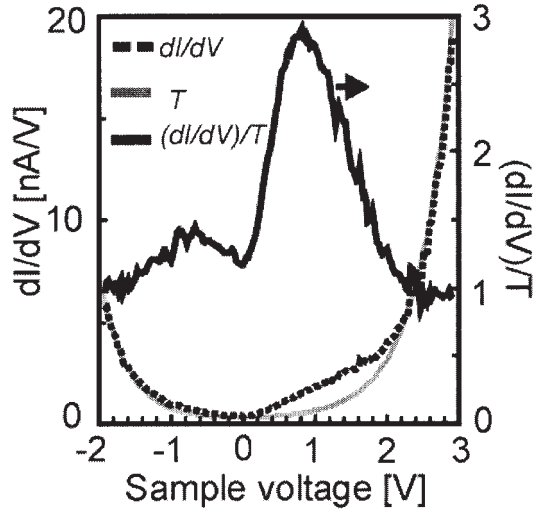

Fig. 2. dI/dV curves measured at layers above the third layer (dots). The set point of $V_s = -0.5$ V, I = 0.5 nA was used and the curve is an average of typically 20 single curves. A fit of the tunneling probability function to the dI/dV curve is also shown (T: grey solid curve). The dI/dV curve normalized by this T, i.e., $(dI/dV)/T$ (black solid curve), reveals a strong peak around +0.8 eV. Also, besides this +0.8 eV peak, a weak peak at −0.6 eV is observed in the $(dI/dV)/T$ curve.

$$J(z,V) \cong \frac{2\pi e}{\hbar}\left(\frac{\hbar^2}{2m}\right)^2 \int_0^{eV} T(z,V,E)\rho_s(E)\rho_t(E-eV)dE$$

Assuming a strong preference for tunneling of electrons with the parallel component of the wave vector equal to zero, the transmission probability can be written in the following way:

$$T(z,V,E) \cong \exp\left[-2z\sqrt{\frac{2m}{\hbar^2}\left(\bar{\phi}+\frac{eV}{2}-E\right)}\right]$$

where $\bar{\phi}$ is the tip and sample average work function, and E is the electron energy.

The dI/dV curves reflect not only the sample surface LDOS but also the tip LDOS and the tunneling probability. In the dI/dV curves, these two contributions show up as an exponential background if the tip LDOS is featureless in the energy range measured. The exact energy position of the LDOS peaks obtained from this method depends strongly on the exponential background. Several methods have been proposed to overcome this problem (Lang, 1986). Ukraintsev (1996) proposed to normalize the dI/dV curves with a tunneling probability function (T) given by:

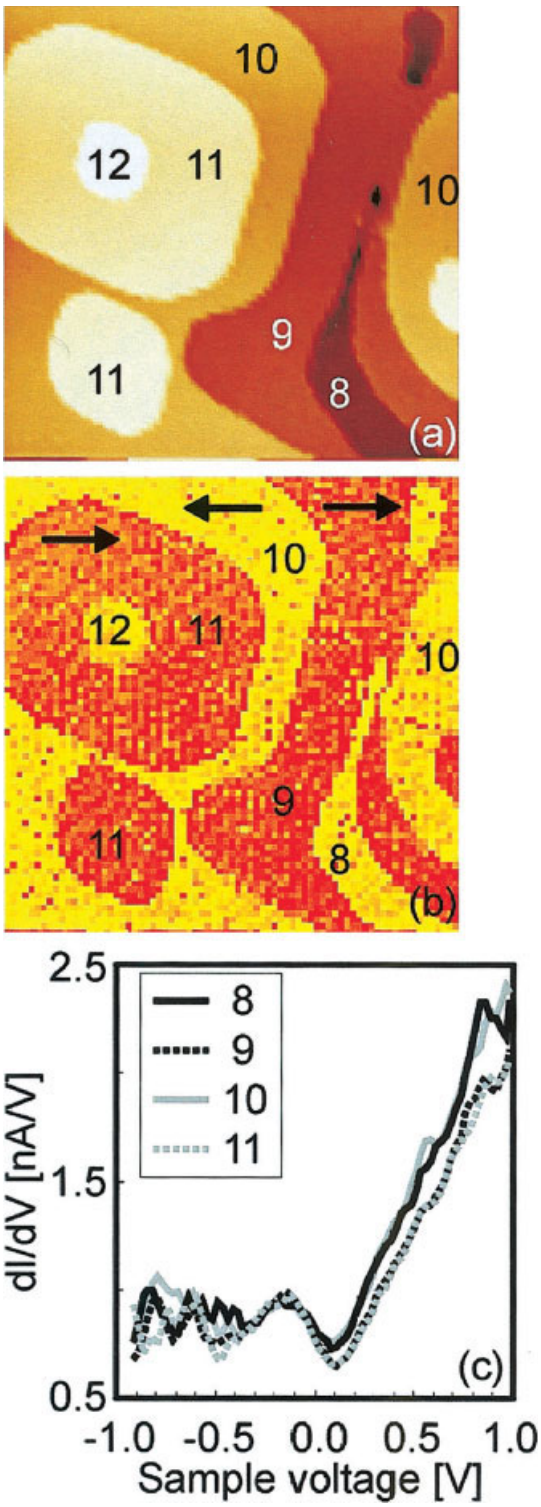

Fig. 3. SP-STM and SP-STS measurements on Fe(001) covered with about 10 ML Mn at 370 K. These measurements were performed with an Fe-coated W tip. (**a**) The topographic image that was obtained at $V_s = -0.5$ V, I = 0.5 nA. Scan size is 100×100 nm^2. Five layers are exposed. The numbers in a and b denote the local thickness of the Mn film. (**b**) The dI/dV map at +0.2 V measured at the same area as a. (**c**) dI/dV curves as a function of the sample bias voltage obtained on the area shown in a. dI/dV curves obtained on even (odd) Mn layers are shown as solid (dashed) curves, which were numerically obtained from $I(V)$ curves measured at a set point of $V_s = -0.5$ V, I = 0.5 nA.

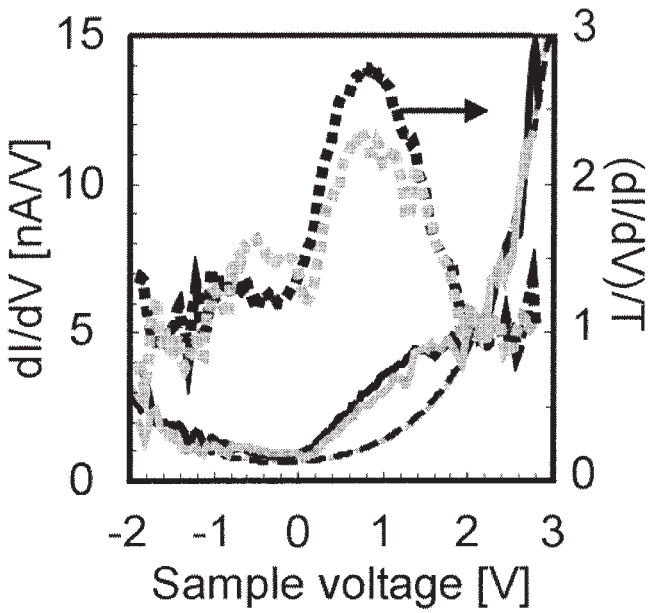

Fig. 4. dI/dV curves normalized by the voltage-dependent tunneling probability function, which were obtained with an Fe-coated W tip on Mn films thicker than three layers. Solid and dotted curves are the dI/dV and the $(dI/dV)/T$ curves, respectively. Tunneling probability function (dashed curves) was obtained by a fit to the dI/dV curve. Black and grey curves are representatives of the odd and the even layers, respectively.

$$T = a_t \exp\left[-2z\sqrt{\frac{2m}{\hbar^2}\left(\bar{\phi} - \frac{eV}{2}\right)}\right] + a_s \exp\left[-2z\sqrt{\frac{2m}{\hbar^2}\left(\bar{\phi} + \frac{eV}{2}\right)}\right]$$

where $z = d$ (a constant tip-sample separation) since the separation is fixed during a spectroscopy measurement. The first (second) term of T describes tunneling from the tip (sample) Fermi level to unoccupied sample (tip) states. a_t and a_s are proportionality coefficients related to the tip-surface effective contact area and are proportional to the tip and sample LDOS at the Fermi level, respectively. Normalizing the dI/dV curves with the function T, we found two different expressions for positive and negative bias voltages:

$$\frac{(dI/dV)}{T} \cong \rho_s(eV)\rho_t(0) \text{ for } \quad V > 0$$
$$\frac{(dI/dV)}{T} \cong \rho_s(0)\rho_t(eV) \text{ for } \quad V < 0$$

This result means that STS is mainly useful to find the empty density of states of the tip or sample while for the occupied density of states the technique quickly looses sensitivity going below the Fermi level.

In order to get magnetic information from the sample surface it is necessary to include the spin orientation of sample and tip in the tunneling current expressions.

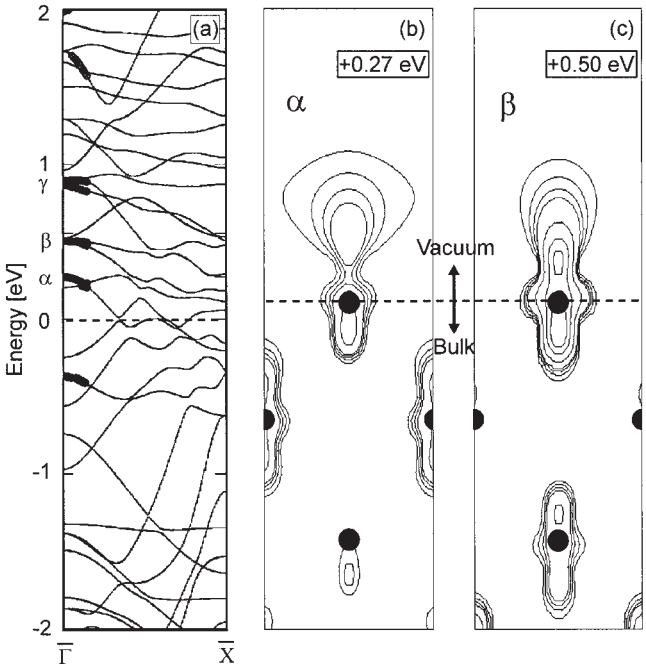

Fig. 5. (**a**) Band structure of an eight-layer Mn(001) slab. The plot shows both "majority" and "minority" bands, which are equivalent for this even-layered antiferromagnetically ordered slab. The magnetization for each layer is defined by the difference in integrated local DOS of the majority and minority bands. Thick black lines: d_z^2-like states around Γ; dashed line: the Fermi level. α, β, and γ could contribute to the experimentally observed +0.8 V peak. (**b,c**) The isocharge density distributions of the α and the β state at the Γ point for two different energies, 0.27 eV and 0.50 eV. Dots and dashed lines indicate atom positions and the boundary between vacuum and bulk, respectively.

The spin-polarization is defined by the difference between the number of electrons in the minority and majority bands integrated up to the Fermi level divided by the total number of electrons. Let us assume that the sample polarization vector ($\boldsymbol{P_s}$) defines the x-axis and lies within the sample surface plane. Then $\boldsymbol{P_s}$ and $\boldsymbol{P_t}$ (tip polarization vector) can be described as follows:

$$\boldsymbol{P_s} = (P_s, 0, 0)$$
$$\boldsymbol{P_t} = (P_t \cos\phi \cos\theta, P_t \cos\phi \sin\theta, P_t \sin\phi)$$

where $0 \leq \phi \leq \pi/2$ is the angle between the tip polarization vector and the sample surface, θ is the angle between the projection of the tip polarization vector on the sample surface and the sample polarization vector. The modulus of the polarization vectors are defined as: $|\boldsymbol{P_i}| \equiv (\rho_{i\uparrow} - \rho_{i\downarrow})/(\rho_{i\uparrow} + \rho_{i\downarrow})$ where i represents tip or sample. Finally, $\rho_{s\uparrow}(\rho_{t\uparrow})$ and $\rho_{s\downarrow}(\rho_{t\downarrow})$ denote spin-up and spin-down sample (tip) LDOS, respectively. The x-y plane is defined by the sample surface and the z axis is perpendicular to it. Now the tunneling current depends also on the dot product of the polarization vectors, $\boldsymbol{P_s} \cdot \boldsymbol{P_t} = |P_s||P_t| \cos\phi \cos\theta$. After including this effect in the differential tunneling conductance, the new expressions for the normalized differential tunneling conductance are:

$$\frac{(dI/dV)}{T} \cong \frac{1}{2}\rho_s(eV)\rho_t(0)\left[1 + \boldsymbol{P_s}(eV)\boldsymbol{P_t}(0)\right] \text{ for } \quad V > 0$$

$$\frac{(dI/dV)}{T} \cong \frac{1}{2}\rho_s(0)\rho_t(eV)\left[1 + \boldsymbol{P_s}(0)\boldsymbol{P_t}(eV)\right] \text{ for } \quad V < 0$$

These equations demonstrate that from the $(dI/dV)/T$ curves it is possible to get not only qualitative information about the sample polarization, for example taking images with contrast between different magnetic domains, but it is also possible to get quantitative information. In the following, we will discuss how to get quantitative information about the sample polarization and the influence of the tip magnetic structure on the SP-STM experiments.

MAGNETIC STRUCTURE AND POLARIZATION OF THE SURFACE OF Mn(001) THIN FILM

SP-STS measurements contain information about the DOS and the relative orientation of the magnetizations of both tip and sample. Therefore, in order to study the magnetic structure of samples, it is favorable to know their electronic structure as measured with a non-magnetic tip. For this purpose, we use a clean W tip. STM/STS measurements on Mn films thicker than four layers are shown in Figure 1. Figure 1a shows an STM topographic image obtained on Fe(001) covered by 7.2 ML of Mn. At each pixel of the topographic image, $I(V)$ curves were measured. The resulting curves are shown in Figure 1c. All curves obtained above the third Mn layer are identical, indicating that the DOS does not change from one layer to the other. This is also clear from Figure 1b, where the dI/dV map shows no contrast between the different terraces.

In order to better identify the different contributions to the dI/dV curves, we performed measurements in a wide voltage range (from −2.0 V up to +3.0 V). These dI/dV curves can be fitted quite accurately by a tunneling probability function (T) (Ukraintsev, 1996). T was obtained by a fit to the curves above +2 V and below −1 V, where the dI/dV curves increase exponentially. The main feature present on the $(dI/dV)/T$ curves is a broad peak at 0.8 eV above the Fermi level and a less pronounced peak below, as can be seen in Figure 2.

For the SP-STS measurements, we deposited between 7–10 nm of Fe at room temperature on the apex of the tips. Figure 3 shows SP-STM/SP-STS measurements obtained with an Fe-coated tip on 10 ML of Mn grown on an Fe whisker. At each pixel of the image, first the tip-sample separation is fixed with a set point of $V_s = -0.5$ V and I = 0.5 nA and the topographic information was measured (Fig. 3a). The numbers on the topographic image denote the local Mn thickness. Subsequently, an $I(V)$ curve was measured. dI/dV curves were obtained numerically. The result is plotted in Figure 3c. The solid and dotted curves were measured on the odd and even layers, respectively. Contrary to the case of the curves measured with a clean W tip, where all the layers show the same amplitude of the dI/dV curves, for the curves measured with Fe-coated tips there is a clear change in the amplitude above the

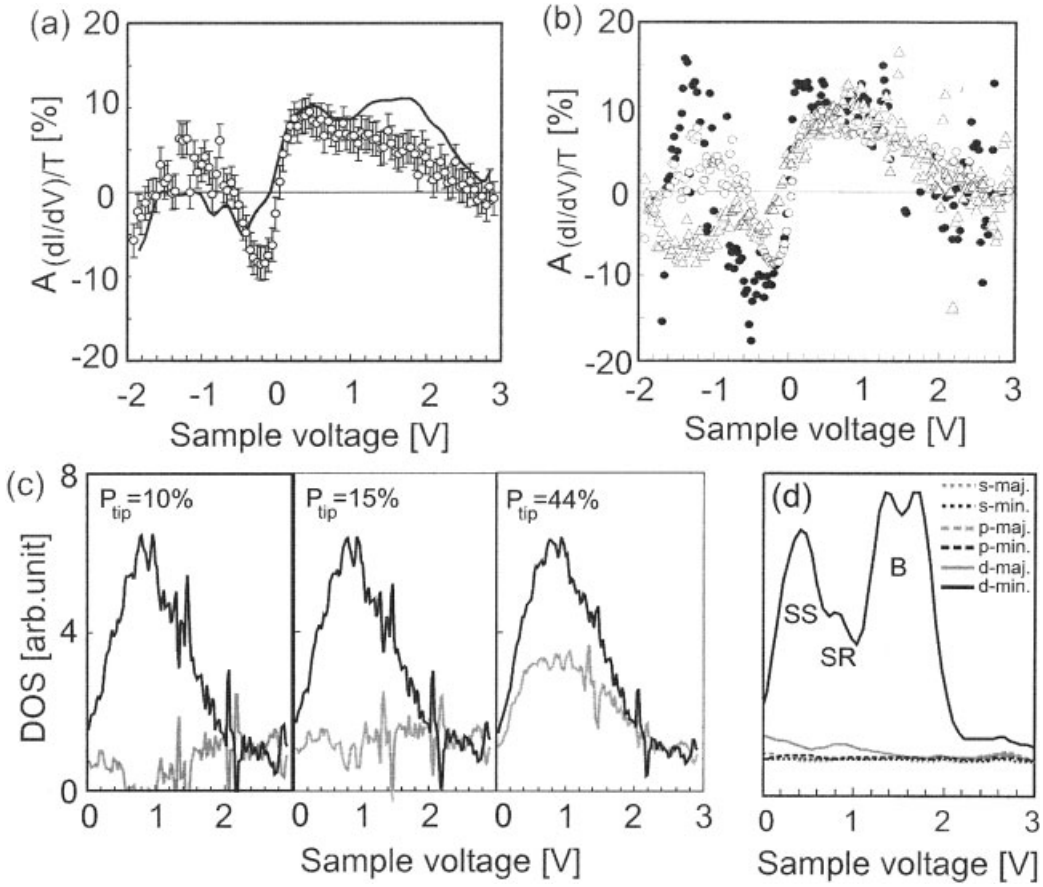

Fig. 6. (**a**) The asymmetry of the *(dI/dV)/T* curves obtained on the even and odd Mn layers as a function of the sample bias voltage. The black solid curve is obtained from the calculated spin-resolved DOS. (**b**) The asymmetry of the *(dI/dV)/T* curves obtained with different set points and different Fe-coated tips. Black dots and triangles were obtained by the same Fe-coated W tip. White dots were obtained by a different Fe-coated W tip. Black and white dots were obtained at a negative voltage set point ($V_s = -0.5$ V, I = 0.5 nA). Triangles were obtained at a positive voltage set point ($V_s = +0.5$ V, I = 0.5 nA). (**c**) The majority (grey) and minority (black) LDOS of Mn(001) were obtained by experimentally obtained *(dI/dV)/T* curves with a tip polarization at the Fermi level of 10, 15, and 44%, respectively. (**d**) The majority (grey) and minority (black) LDOS of Mn(001) obtained by band structure calculations. SS, SR, and B denote surface states, a surface resonance, and bulk states, respectively.

Fermi level between the curves measured on the even and odd layers.

In Figure 3b, we show a dI/dV map constructed with the value of the dI/dV curves at +0.2 V. This map clearly shows that the contrast oscillates with a period of two layers. Although the odd layers (9 and 11) are darker than the even layers (8, 10, and 12) in this particular dI/dV map, this is not always the case; with other tips the contrast is reversed. With the actual experimental setup, it is not possible to determine the absolute magnetization orientation of the tip. We explain the alternating contrast in the dI/dV maps obtained with the Fe-coated tips by the layered antiferromagnetic magnetization of the Mn(001) layers.

We will apply the normalization procedure by the function T explained previously with the dI/dV curves measured with the Fe-coated tips. Figure 4 shows *(dI/dV)/T* curves averaged over 30 single curves measured with an Fe-coated tip. The curves measured on even layers (grey line) and odd layers (black line) show two peaks at the same energies as the peaks obtained with the clean W tips. The main difference of the curves measured with the clean W tips is that now the amplitude of both peaks oscillates with a period of two layers and the curves measured on the even and odd layers cross at the Fermi level.

Natural occurring *3d* metals with bcc structure such Fe and Cr have a surface state at the (001) surface. On the other hand, Mn, which is between Fe and Cr in the periodic table, has a complicated bulk structure. An open question is whether an artificial bct Mn(001) thin film also shows a surface state. In order to determine the nature of the spin-dependent peaks present in the *(dI/dV)/T* curves (Fig. 4), band structure calculations were carried out by Heijnen (Yamada et al., 2003b) of the Theoretical Physics Department at the Radboud University of Nijmegen using the Vienna Ab initio Simulation Program (VASP). It is based on spin density functional theory and the projected augmented wave (PAW) method (Blöchel, 1994; Kresse and Joubert, 1999) with non-local corrections to the exchange and correlation taken into account by a generalized gra-

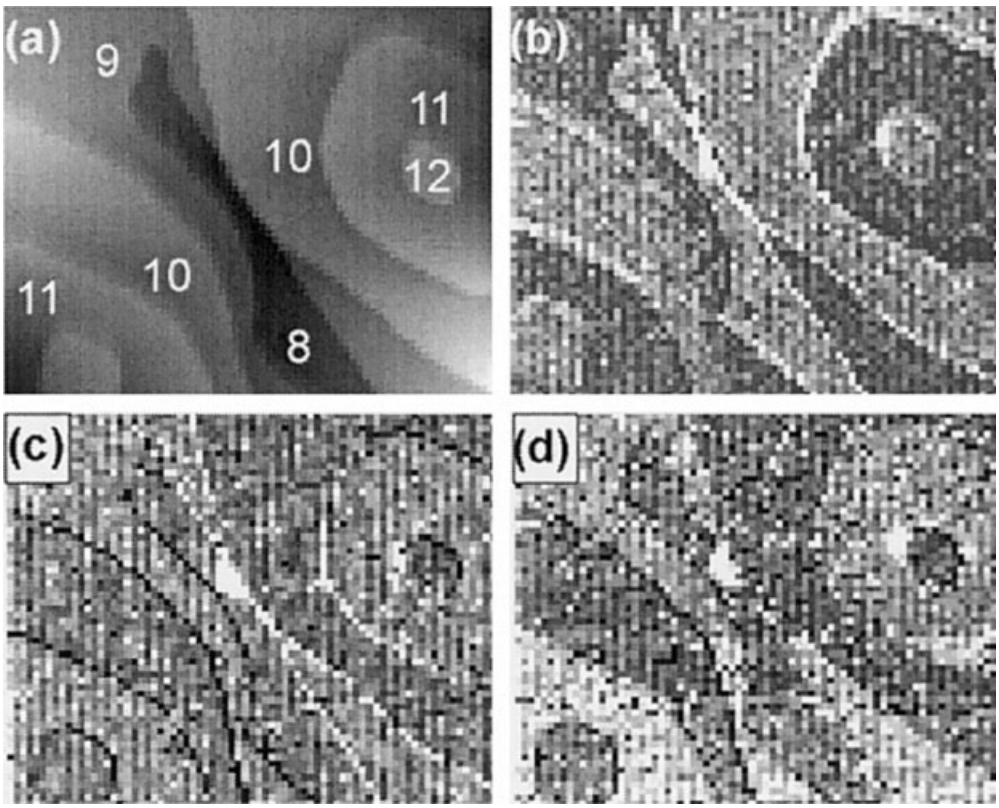

Fig. 7. SP-STS measurements on Fe(001) covered with 9.5 ML Mn at 370 K showing a reversal of the magnetic contrast after pulsing the tip. (**a**) A topographic image measured at a set point of $V_s = -0.5$ V, I = 0.5 nA. Scan size is 100×80 nm^2. Five different levels are exposed on the surface; the numbers denote the local thickness of the Mn film. (**b–d**) dI/dV maps at +0.2 V measured at the same area as a. Between b–d, the tip was moved 500 nm away from this area and a voltage pulse was applied.

dient approximation (GGA). An eight-layer slab with the experimental values for the in-plane (2.87 Å) and out-of-plane (2×1.64 Å) lattice constants was used; an antiferromagnetic stacking of Mn(001) layers was assumed (Tulchinsky et al., 2000). Figure 5a shows the "majority" and "minority" bands obtained in the calculation for 8-Mn layers. In the plot, the bands with the largest d_z^2 character at the Γ point are marked with thick black lines.

Three bands are possible candidates for the experimentally observed empty state peak; the band called α at 0.27 eV, β at 0.50 eV, and γ at 0.87 eV above the Fermi level. The calculations show the DOS at the Mn(001) surface while the tip detects the DOS in the vacuum at the tip position. To check the distribution of each state in the vacuum, the surface charge density distribution was calculated and is shown in Figure 5b and c for bands α and β, which exhibit a surface state–like behavior. The γ band displays a strong decay into the vacuum.

The width of the +0.8 V peak in $(dI/dV)/T$ is about 1 V (Fig. 4). This width is larger than the peak obtained on Fe(001) (0.13 eV) (Stroscio et al., 1995) and Cr(001) (0.2 eV at RT) (Kleiber et al., 2000). One possible explanation is that in our case the peak at +0.8 eV is produced by two surface states α and β. The difference between the calculated peak energies and the experimental peak energy is attributed to the limitations of the calculation.

Once the spin-polarized tunneling contributions to the electronic spectra have been identified, we will try to extract quantitative information from them. Since the $(dI/dV)/T$ shows the sample (tip) DOS multiplied by the tip (sample) DOS at the Fermi energy for $V > 0$ ($V < 0$), in principle it is possible to obtain the sample polarization. The asymmetry of the normalized tunneling conductance, $A_{(dI/dV)/T}$, defined as follows:

$$A_{(dI/dV)/T} = \frac{(dI/dV)_{even}/T_{even} - (dI/dV)_{odd}/T_{odd}}{(dI/dV)_{even}/T_{even} + (dI/dV)_{odd}/T_{odd}}$$

corresponds to the sample (tip) polarization as a function of the sample bias voltage multiplied by the tip (sample) polarization at the Fermi energy for V > 0 (V < 0), i.e. $A_{(dI/dV)/T} = P_s(V)P_{tip}(E_F)$ for V > 0 and $P_{tip}(V)P_s(E_F)$ for V < 0 (Yamada et al., 2003a). Also, T_{odd} and T_{even} denote the tunneling probability functions obtained from dI/dV_{odd} and dI/dV_{even}, respectively. T_{odd} and T_{even} are not identical. By the fitting different tip-sample separations are obtained due to spin-polarized tunneling, e.g., 0.90 nm for T_{odd} and 0.92 nm for T_{even}, assuming the same averaged work function on both terraces.

The asymmetry curves shown in Figure 6a,b were obtained from dI/dV curves showing spin-dependent peaks with the maximum magnetic contrast, which

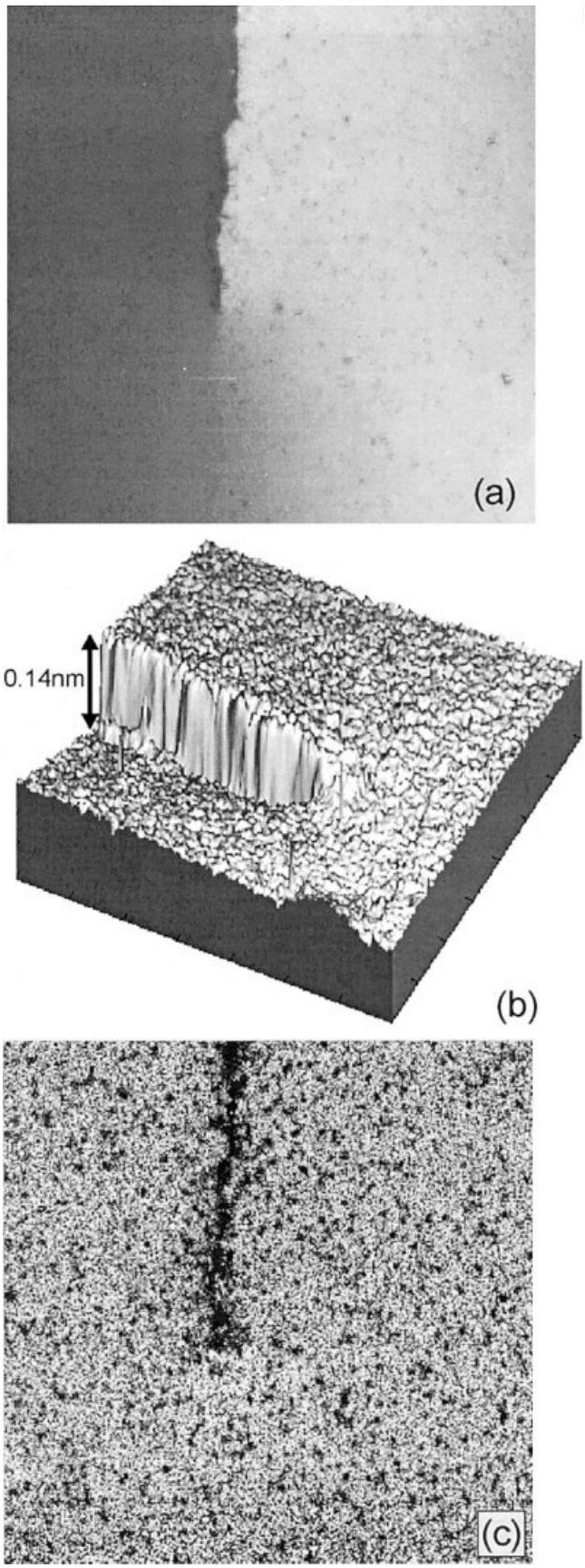

were obtained from different voltage set points and different Fe-coated W tips. The $A_{(dI/dV)/T}$ is at maximum 10% below and above the Fermi energy, while the sign changes at the Fermi level. The changes in the fitting parameters for T produce errors in the asymmetry of 2% (error bars in Fig. 6a). The calculated polarization of the Mn(001) surface divided by a 15% tip polarization is shown as a solid curve in Figure 6a. The calculated curve fits to the experimentally obtained asymmetry curve except around +2 V where the calculation include bulk states while SP-STS only detects surface LDOS. In order to show the reproducibility of this method, we show in Figure 6b the asymmetry obtained in different experiments. The asymmetries plotted with dots and triangles were obtained with the same Fe-coated W tip and different set points (positive and negative bias voltage respectively); the one represented by circles was measured with a different Fe-coated W tip. These tips showed the maximum value on the asymmetry of the $(dI/dV)/T$ curves, which are assumed to be parallel (or anti-parallel) between the tip and the sample magnetization direction. This plot demonstrates that the asymmetry obtained by the normalized conductance does not depend on the set point or on the tip.

We will focus now on the analysis of the asymmetries above the Fermi level that is the energy range where STS is sensitive to the sample DOS. For the positive sample bias voltage, the $(dI/dV)/T$ curves for the odd and even layers can be described as follows:

$$\frac{(dI/dV)_{even}}{T_{even}} = \left(D^{\uparrow}_{tip}(E_F)D^{\min}_{Mn}(V) + D^{\downarrow}_{tip}(E_F)D^{maj}_{Mn}(V)\right)$$
$$\frac{(dI/dV)_{odd}}{T_{odd}} = \left(D^{\uparrow}_{tip}(E_F)D^{maj}_{Mn}(V) + D^{\downarrow}_{tip}(E_F)D^{\min}_{Mn}(V)\right)$$

$D^{\uparrow}_{tip}(E_F)(D^{\downarrow}_{tip}(E_F))$ indicates the LDOS at the Fermi level for the majority (minority) bands of the Fe-coated W tips. Since the tip is ferromagnetic, majority-spin and minority-spin bands of the Fe-coated W tips are defined as spin-up and spin-down. $D^{maj}_{Mn}(V)$ $(D^{min}_{Mn}(V))$ indicates the LDOS at the energy V above the Fermi level for the majority (minority) bands of the sublattices of antiferromagnetic bct Mn films. For a layered antiferromagnetic material, the occupation of the majority and minority band switches from spin-up to spin-down electrons in every layer. For this reason we will use majority and minority for the sample. Assuming that spin-up (-down) electrons from the tip will tunnel into the minority (majority) spin bands of the odd Mn layers and into the majority (minority) spin bands of the even Mn layers without spin flipping, we can describe the asymmetry as

$$A_{(dI/dV)/T} = P_T(E_F)P_s(E_F + eV), \quad where\ V > 0$$

Fig. 8. (**a**) An STM topographic image (70 × 70 nm^2) obtained on the Fe(001) whisker clean surface at a screw dislocation. (**b**) The STM image of a in a three-dimensional mode. (**c**) dI/dV map at +0.2 V obtained simultaneously with the image shown in a taken with a set point of $V_s = -0.6$ V, I = 0.5 nA.

Using these three equations the spin-resolved LDOS of the Mn(001) can be experimentally obtained as follows:

$$D_{Mn}^{maj} = \frac{1}{C}\left(1 - \frac{A_{(dI/dV)/T}}{P_T}\right)\left[\frac{(dI/dV)}{T}\right]_{ave}$$

$$D_{Mn}^{min} = \frac{1}{C}\left(1 + \frac{A_{(dI/dV)/T}}{P_T}\right)\left[\frac{(dI/dV)}{T}\right]_{ave}$$

where $[(dI/dV)/T]_{ave}$ is the average of $(dI/dV)_{odd}/T_{odd}$ and $(dI/dV)_{even}/T_{\text{even}}$. C is the sum of $D_{tip}^{\uparrow}$ and $D_{tip}^{\downarrow}$ and P_T is the tip polarization. Using the experimentally obtained $(dI/dV)/T$ and $A_{(dI/dV)/T}$, the spin-resolved sample LDOS can be obtained as is shown in Figure 6c for three different tip polarizations. For comparison, the calculated spin-resolved LDOS for the sample is shown in Figure 6d. Comparing the experimentally obtained results with different tip polarizations, we conclude that the best fit between the experimentally obtained majority LDOS and the calculated majority LDOS is obtained with a tip polarization of 18 ± 5%. With this tip polarization, we obtain a Mn surface polarization of 60 ± 16% at +0.8 eV.

MODIFICATION OF THE TIP MAGNETIZATION

In the present section, we will describe a method to change the magnetization of the tip by applying voltage pulses (Yamada et al., 2003c). During constant current STM topographic measurements (typically, $V_s = +1$ V, I = 0.1 nA), we increased the bias voltage from 1 to 10 V in 60 μs with the feedback on. The feedback loop is too slow to keep the tunneling current constant and it needs around 15 ms to recover the original value of the tunneling current (0.1 nA). During these 15 ms, the I/V converter is saturated and the output is at the maximum value that it is able to measure (3.7 nA); during this time, the current density increases drastically and the tip structure is modified.

Figure 7 shows the dependence of the alternating contrast in the dI/dV maps on the tip condition. Figure 7a shows a topographic image; the numbers denote the local thickness of the Mn film. Figure 7b shows the original contrast (5%) obtained with the spin-polarized tip. The alternating contrast between the even and odd Mn layers is clear in the dI/dV map. After taking this dI/dV map, we moved the tip 0.5 μm away from this area of the sample and we applied a voltage pulse. Then the tip was moved back to the original area and another dI/dV map was measured; the result is shown in Figure 7c; in this case, the contrast is almost negligible (<1%). After this measurement, we moved the tip away from the area and we applied another voltage pulse. Figure 7d was measured after this second voltage pulse. In this dI/dV map the contrast is recovered but is inverted (−6%) with respect to the one originally obtained (Fig. 7b). From this experiment, it is clear that the magnetic contrast depends strongly on the tip condition and this can be altered in a random way with voltage pulses.

MAGNETIC STRUCTURE AROUND A SCREW DISLOCATION IN AN ANTIFERROMAGNETIC FILM

Occasionally, we found screw dislocations on the Fe(001) surface. In Figure 8a,b, we show STM images

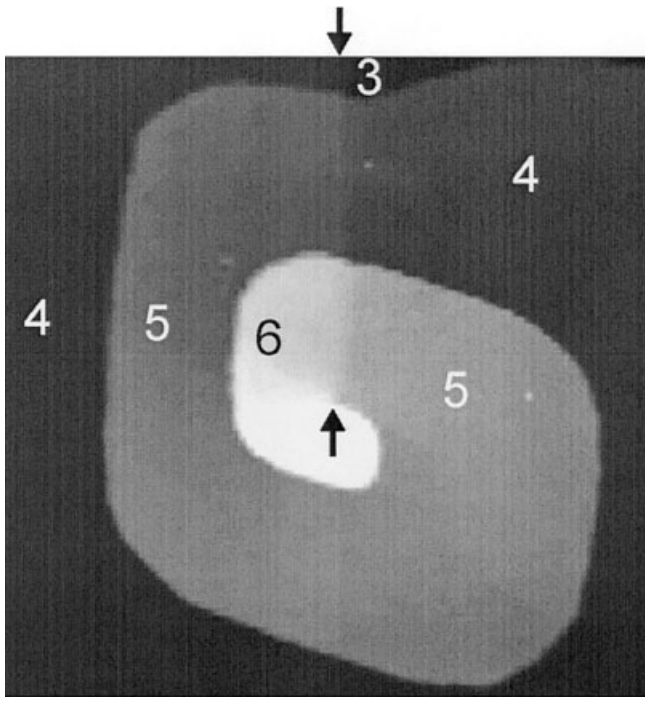

Fig. 9. An STM topographic image obtained on an Fe(001)-screw-dislocation covered with 4.5 ML Mn at 370 K at a set point of $V_s = -0.5$ V, I = 0.5 nA (100 × 100 nm^2). The arrows indicates the position of the screw dislocation on the Fe(001) surface. Numbers denote local thickness of the Mn film.

obtained at a screw dislocation on the Fe(001) surface. The Fe(001) surface exhibits a surface state of d_z^2 character at 0.17 eV above the Fermi level (Bischoff et al., 2003; Stroscio et al., 1995). Figure 8c shows a dI/dV map at +0.2 V obtained in the same area as the topography shown in Figure 8a. A black line is observed at the position of the step edge indicating the disappearance of the iron surface state; the small black dots on the terraces indicate the position of contaminants. Since Fe has a ferromagnetic character, no magnetic structure is observed around the screw dislocation in contrast to the screw dislocation on the antiferromagnetic Cr(001) surface (Ravlic et al., 2003).

This lack of magnetic structure changes when antiferromagnetic Mn layers are deposited on the screw dislocation. The Mn layers grow with a spiral structure. In Figure 9, we show an STM image taken on 4.5 ML of Mn deposited on an Fe screw dislocation. The numbers indicate the Mn local coverage and were determined by measuring STS spectra since the third Mn layer has a characteristic dI/dV curve (Yamada et al., 2002).

The dI/dV map at +0.4 V obtained around the screw dislocation shows magnetic contrast as can be seen in Figure 10a. A detailed analysis of the dI/dV map reveals that several amplitudes of magnetic contrast are present (marked from A to G in Fig. 10a).

In Figure 10b, we show individual dI/dV curves obtained at the areas marked "A–G" in Figure 10a. The maximum magnetic contrast is obtained between the dI/dV curves measured on the fourth (A) and fifth (B)

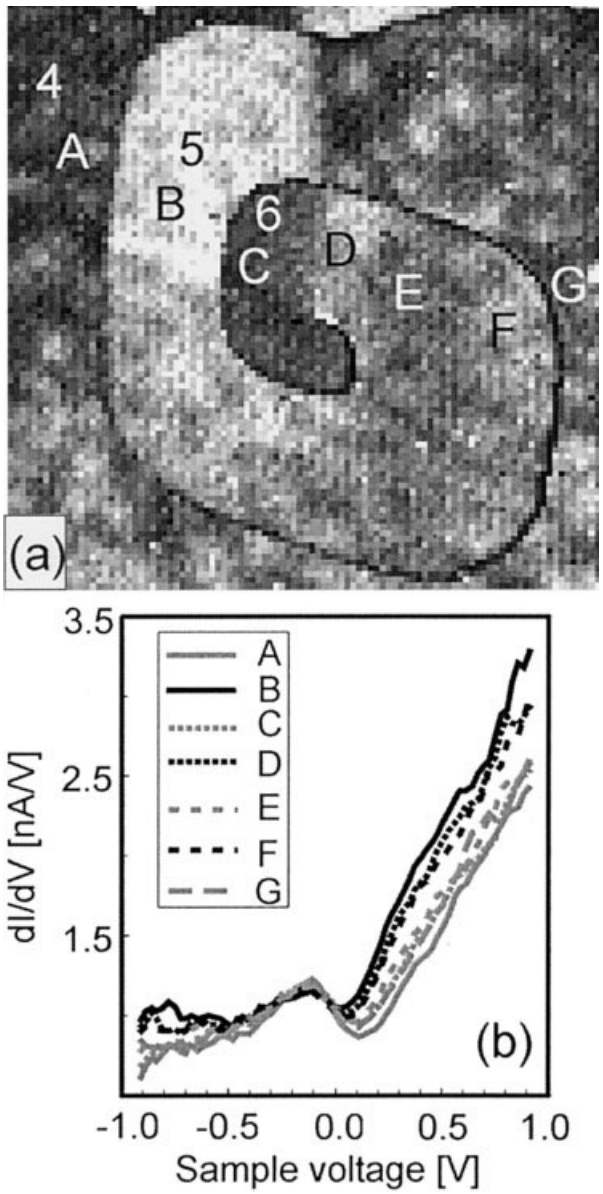

Fig. 10. (**a**) SP-STS image (a dI/dV map at +0.4 V) obtained at the same area as Figure 9 at a set point of $V_s = -0.5$ V, I = 0.5 nA with a magnetic tip (100×100 nm^2). Numbers of 4–6 denote stacking numbers of Mn layers. (**b,c**) dI/dV curves obtained at each area of A–G in a.

Mn layers (i.e., $A_{AB} = ((dI/dV)_B - (dI/dV)_A)/((dI/dV)_B + (dI/dV)_A) \sim 20\%$ for $V > 0$). Conversely, the minimum contrast is obtained between the dI/dV curves measured on C and D areas ($A_{CD} \sim 12\%$ for $V > 0$).

It is very difficult to calculate the magnetic structure of the Mn layers around the screw dislocation but we can estimate the relative orientation of the in-plane magnetization of the different areas marked from A to G. The dI/dV curves measured in the odd and even Mn layers can be described as follows

$$\left(\frac{dI}{dV}\right)_{odd} = \frac{dI_0}{dV}(1 + P_{tip}P_s \cos\theta)\exp(2\kappa\Delta z \cos\theta) \quad (1)$$

$$\left(\frac{dI}{dV}\right)_{even} = \frac{dI_0}{dV}(1 + P_{tip}P_s \cos(\theta+\pi)) \times \exp(2\kappa\Delta z \cos(\theta+\pi)) \quad (2)$$

where dI_0/dV denotes the non-spin polarized term of dI/dV, i.e., $dI_0/dV = \frac{1}{2}\rho_{tip}\rho_s \exp(-2\kappa z)$, where $\rho_{tip}(\rho_s)$ denotes the tip (sample) DOS, z the tip-sample distance, κ the decay length. P_{tip} (P_s) denotes the tip (sample) polarization, θ the angle between the tip and the sample magnetizations, and Δz the spin-dependent tip-sample separation. Although P_{tip} and P_s are functions of the sample bias voltage only, Δz depends on the spin polarization in the whole energy window set by the bias voltage, as well as on the spin-polarization of the tip and the relative angle of the magnetization vectors.

Experimentally it has been determined that the spin-dependent tip-sample separation (Δz) is 0.1 Å (Yamada et al., 2003b) for the curves showing the maximum contrast. Using equations (1) and (2) and assuming that the tip and sample magnetizations are parallel ($\theta = 0$), the calculated asymmetry ($A^{cal} = ((dI/dV)_{odd} - (dI/dV)_{even})/((dI/dV)_{odd} + (dI/dV)_{even})$ is 0.2 for the dI/dV curves presenting the highest contrast on Mn layers grown on flat areas of the Fe whisker. For the Mn layers grown on the screw dislocation, we found that the maximum contrast occurs between the areas marked as A and B and the value of the asymmetry is ~ 0.2, which is the maximum value of the magnetic contrast obtained on the Mn(001) layers, for a bias voltage of +0.3 V. Using these values, we can assume that the magnetizations in areas A and B are parallel (antiparallel) to the tip magnetization. Regions marked in Figure 10a as A, C, and G are on the even Mn layers (fourth and sixth), and areas marked as B, D, E, F are on the odd Mn layers (fifth). We also know that the even and odd Mn layer tend to be antiferromagnetically coupled. In order to estimate the relative orientation of the magnetization in the different areas (C–G) in relation to B, we can define a function $f(\alpha) = (dI/dV)_i/(dI/dV)_B$, where α is the angle between the magnetization of the different domains and i denotes the domain (C–G). Due to the tendency of antiferromagnetic coupling between the odd and even Mn layers, α will change by π from the areas in the even and odd layers. Therefore, we will have two functions $f(\alpha)$, one for the odd layers:

$$f_{odd}(\alpha) = \frac{(dI/dV)_i}{(dI/dV)_B} = \frac{(1 + 0.1\cos\alpha)\exp(0.2\kappa\cos\alpha)}{1.1\exp(0.2\kappa)}$$

where i = D, E, F

and one for the even layers:

$$f_{even}(\alpha) = \frac{(dI/dV)_i}{(dI/dV)_B} = \frac{(1 + 0.1\cos(\alpha+\pi))\exp(0.2\kappa\cos(\alpha+\pi))}{1.1\exp(0.2\kappa)}$$

where $i = \mathrm{C}, \mathrm{G}$

Using the dI/dV curves measured experimentally in the different areas, we can determine the value of the

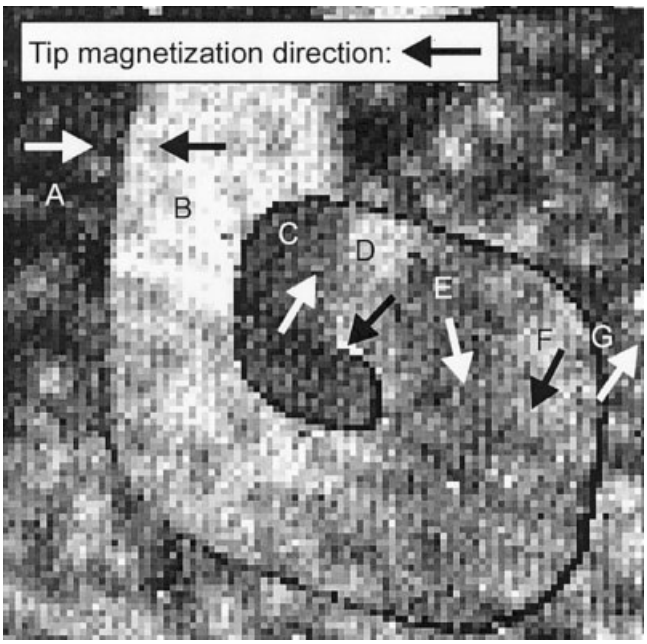

Fig. 11. The same dI/dV map shown in Figure 10 with local magnetization directions calculated from the asymmetry of the dI/dV curves.

$f(\alpha)$ functions and from that value we can extract the value of the angle α. We found that the magnetization in area C makes an angle of 239° with respect to the magnetization in B. For D, we found 47°, 103° for E, 63° for F, and 235° for G. The obtained magnetizations are plotted by arrows in Figure 11.

Figure 12a shows a topographic image of 400 × 333 nm^2 represented in a differentiated mode in order to make visible all the structural details. The numbers denote the local Mn thickness. Fe steps, with a step height of 0.02 nm, show up on the surface as white faint lines, which have been surrounded by black thin lines to guide the eye. In Figure 12b, we show a mosaic composed by 12 dI/dV maps at +0.1 V obtained in several areas of the topography shown in Figure 12a. The third Mn layer appears brighter than the other layers due to a different DOS not related to the magnetic properties. The obtained magnetization directions are shown with arrows on the topography presented in Figure 12a. Although the right-hand side of the image reveals a true antiferromagnetic coupling between the layers, the presence of the screw dislocation rotates the magnetization directions. A clear example of this influence are the two islands marked with white squares in Figure 12a. Both islands are 5-ML-thick but the magnetization directions of these islands make a 90° angle.

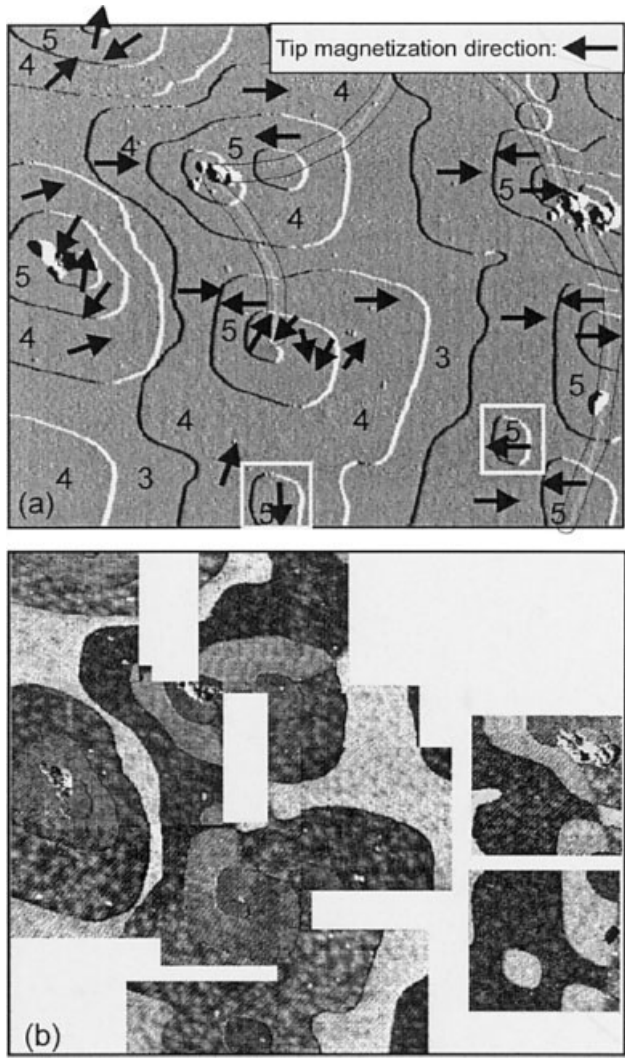

Fig. 12. (**a**) SP-STM topographic image in a differential mode obtained with a magnetic tip on 4.5 ML Mn on Fe(001) at 370 K at a set point of $V_s = -0.5$ V, I = 0.5 nA (400 × 333 nm^2). Hidden Fe steps and a hidden Fe dislocation are observed as white curves surrounded by black curves. Numbers in a denote the stacking numbers of the Mn layers. Arrows denote relative angles of magnetization directions. Boxes show fifth Mn layers with different magnetization directions. (**b**) Twelve dI/dV maps at +0.1 V obtained at several areas in a. Due to the thermal drift, the 12 dI/dV maps were not connected perfectly.

CONCLUSIONS

We have shown that by combining a detailed analysis of the SP-STS measurements with spin-resolved band structure calculations, it is possible to obtain quantitative information about the polarization of surfaces with very high resolution. We also discussed an experimental approach for modifying the tip magnetization direction. Finally, we have shown that SP-STM/SP-STS experiments allow us to study in detail the magnetic structure around isolated defects on surfaces, like a screw dislocation. These defects are not accessible with other spatially averaging techniques. We have shown that, even for a complicated situation like a screw dislocation in an antiferromagnetic film, the direction of the sample magnetization can be determined.

ACKNOWLEDGMENTS

A.L.V.P. acknowledges the financial support by the Ministerio de Educación y Ciencia (MEC) through Project No. FIS2004-01026. T.K.Y. acknowledges Grant-in-Aid for JSPS Fellows. H.v.K. acknowledges a DVF from the

International Research Center for Experimental Physics (IRCEP) at the Queen's University, Belfast (Ireland).The authors thank Dr. D.T. Pierce for supplying the Fe whiskers. This work was supported by the Stichting voor Fundamenteel Onderzoek der Materie (FOM), which is funded by the Nederlandse Organisatie voor Wetenschappelijk Onderzoek.

REFERENCES

Alvarado SF, Renaud P. 1992. Observation of spin-polarized-electron tunneling from a ferromagnet into GaAs. Phys Rev Lett 68:1387–1390.

Bardeen J. 1961. Tunneling from a many-particle point of view. Phys Rev Lett 6:57–59.

Binnig G, Rohrer H, Gerber Ch, Weibel E. 1982. Surface studies by scanning tunneling microscopy. Phys Rev Lett 49:57–61.

Bischoff MMJ, Yamada TK, van Kempen H. 2003. Local electronic structure of Fe(001) surfaces studied by scanning tunneling spectroscopy. Phys Rev B 68:045422-1–045422-7.

Blöchel PE. 1994. Projector augmented-wave method. Phys Rev B 50:17953–17979.

Bode M, Getzlaff M, Wiesendanger R. 1998. Spin-polarized vacuum tunneling into the exchange-split surface state of Gd(0001). Phys Rev Lett 81:4256–4259.

Heinze S, Bode M, Kubetzka A, Pietzsch O, Nie X, Blügel S, Wiesendanger R. 2000. Real-space imaging of antiferromagnetism on the atomic scale. Science 288:1805–1808.

Kleiber M, Bode M, Ravlic R, Wiesendanger R. 2000. Topology-induced spin frustrations at the Cr(001) surface studied by spin-polarized scanning tunneling spectroscopy. Phys Rev Lett 85:4606–4609.

Kresse G, Joubert D. 1999. From ultrasoft pseudopotentials to the projector augmented-wave method. Phys Rev B 59:1758–1775.

Lang ND. 1986. Spectroscopy of single atoms in the scanning tunneling microscope. Phys Rev B 34:5947–5950.

Prins MWJ, Jansen R, van Kempen H. 1996. Spin-polarized tunneling with GaAs tips in scanning tunneling microscopy. Phys Rev B 53:8105–8113.

Ravlic R, Bode M, Kubetzka A, Wiesendanger R. 2003. Correlation of dislocation and domain structure of Cr(001) investigated by spin-polarized scanning tunneling microscopy. Phys Rev B 67:174411-1–174411-11.

Stroscio JA, Pierce DT, Davies A, Celotta RJ, Weinert M. 1995. Tunneling spectroscopy of bcc(001) surface states. Phys Rev Lett 75:2960–2963.

Suzuki Y, Nabhan W, Tanaka K. 1997. Magnetic domains of cobalt ultrathin films observed with a scanning tunneling microscope using optically pumped GaAs tips. Appl Phys Lett 71:3153–3155.

Tulchinsky DA, Pierce DT, Davies AD, Stroscio JA, Unguris J, Celotta RJ. 2000. Growth and magnetic oscillatory exchange coupling of Mn/Fe(001) and Fe/Mn/Fe(001). J Magn Magn Mater 212:91–100.

Ukraintsev VA. 1996. Data evaluation technique for electron-tunneling spectroscopy. Phys Rev B 53:11176–11185.

Vázquez de Parga AL, Alvarado SF. 1994. Magnetic circular dichroism in cobalt films observed with scanning tunneling microscope excited fluorescence. Phys Rev Lett 72:3726–3729.

Wiesendanger R, Güntherodt HJ, Güntherodt G, Gambino RJ, Ruf R. 1990. Observation of vacuum tunneling of spin-polarized electrons with the scanning tunneling microscope. Phys Rev Lett 65:247–250.

Wulfhekel W, Kirschner J. 1999. Spin-polarized scanning tunneling microscopy on ferromagnets. Appl Phys Lett 75:1944–1946.

Yamada TK, Bischoff MMJ, Mizoguchi T, van Kempen H. 2002. STM and STS study of ultrathin Mn layers on Fe(001). Surf Sci 516:179–190.

Yamada TK, Bischoff MMJ, Heijnen GMM, Mizoguchi T, van Kempen H. 2003a. Origin of magnetic contrast in spin-polarized scanning tunneling spectroscopy: experiments on ultra-thin Mn films. Jpn J Appl Phys 42:4688–4691.

Yamada TK, Bischoff MMJ, Heijnen GMM, Mizoguchi T, van Kempen H. 2003b. Observation of spin-polarized surface states on ultrathin bct Mn(001) films by spin-polarized scanning tunneling spectroscopy. Phys Rev Lett 90:056803-1–056803-4.

Yamada TK, Bischoff MMJ, Mizoguchi T, van Kempen H. 2003c. Use of voltage pulses to detect spin-polarized tunneling. Appl Phys Lett 82:1437–1439.